Origin of a Tetragonal $BiFeO_3$ Phase with a Giant *c/a* Ratio on $SrTiO_3$ Substrates

*Huajun Liu, Ping Yang, Kui Yao, Khuong Phuong Ong, Ping Wu, and John Wang**

A tetragonal $BiFeO_3$ phase with giant *c/a* of approximately 1.25 has been of great interest recently as it potentially possesses a giant polarization and much enhanced electromechanical response. This super-tetragonal phase is known to be a stable phase only under high compressive strains of above approximately 4.5%, according to first principle calculations. However, in previous work, this super-tetragonal $BiFeO_3$ phase was obtained in films deposited at high growth rate on $SrTiO_3$ substrates with compressive strain of only around 1.5%. By detailed structure analysis using high resolution synchrotron X-ray diffraction, atomic force microscopy, and transmission electron microscopy, the parasitic β-Bi_2O_3 phase is identified as the origin inducing the formation of super-tetragonal $BiFeO_3$ phase on $SrTiO_3$ substrates. In addition, ab initio calculations also confirm that this super-tetragonal phase is more stable than monoclinic phase when Bi_2O_3 is present. Using Bi_2O_3 as a buffer layer, an alternative route, not involving strain engineering, is proposed to stabilize this promising super-tetragonal $BiFeO_3$ phase at low growth rates.

1. Introduction

$BiFeO_3$ (BFO) is one of the most interesting multifunctional materials to have been extensively studied in recent years.[1] It shows robust ferroelectric, magnetic, piezoelectric, and optical properties.[2] In particular, the electromagnetic coupling in BFO promises the electrical control of magnetization and vice versa, which may lead to several new memory and device revolutions.[3] In addition, the close matching of its band gap to visible light spectrum adds on further potential in photovoltaic devices.[4]

To develop high quality BFO films for device applications, epitaxial strains from the substrate have been widely employed to tune the crystal phase and thereby the physical behavior, a technique known as "strain engineering".[5] In epitaxial thin films, the BFO crystal structure could be stabilized in several different crystal systems, including monoclinic (M_A, M_B, and M_C), tetragonal, rhombohedral, orthorhombic, and triclinic arrangements. Indeed, all the crystal systems except cubic and hexagonal are included, driving BFO as an ideal model material for strain-engineering study. Bulk BFO crystal shows a rhombohedral structure with space group *R3c*.[6] A compressive strain of approximately 1.5% from $SrTiO_3$ (STO) substrate has been shown to result in a tetragonal BFO phase with small *c/a* ratio of around 1.04 at film thicknesses of less than 50 nm;[7] At film thicknesses above 50 nm and below 700 nm, BFO lattice partially relaxes to a monoclinic M_A phase; finally, for very thick film of around 2 μm it fully relaxes to a bulk rhombohedral structure.[8,9] Larger compressive strains of around 4.5% elongate the out-of-plane dimension of the BFO lattice greatly, leading to a monoclinic structure with giant *c/a* approximately 1.25, as demonstrated by polarized Raman study.[10,11] At compressive strain of above 4.5%, a super-tetragonal BFO phase with similar giant *c/a* could be formed according to first principle calculations.[12] In a recent experimental report of BFO films deposited on $LaAlO_3$ (LAO) substrate, undoped BFO films show an M_C structure while only barium-doped BFO films exhibit a strictly super-tetragonal phase.[9] More recently, two triclinic phases were identified as low symmetry phases at the morphotropic phase boundary (MPB) in a phase-mixed BFO film.[13] Tensile strain, on the other hand, leads to a shrinkage of the out-of-plane dimension and elongation of the in-plane length of BFO lattice. Monoclinic M_B phase could be formed under small tensile strain. An extremely large tensile strain could lead to an orthorhombic phase with only in-plane polarization, which would be of considerable value if it could be demonstrated experimentally.[14]

Among all these phases existing in the epitaxial BFO thin films, the super-tetragonal phase with giant *c/a* is of particular interest as it shows an enhanced electromechanical response at MPB.[15] Also, it was predicted to exhibit giant polarization

H. Liu, Prof. J. Wang
Department of Materials Science and Engineering
National University of Singapore
Singapore 117574, Singapore
E-mail: msewangj@nus.edu.sg
H. Liu, Dr. K. Yao
Institute of Materials Research and Engineering
A*STAR (Agency for Science, Technology and Research)
Singapore 117602, Singapore
Dr. P. Yang
Singapore Synchrotron Light Source National University of Singapore
5 Research Link, 117603, Singapore
Dr. K. P. Ong, Dr. P. Wu[+]
Institute of High Performance Computing
1 Fusionopolis Way,# 16-16 Connexis, Singapore 138632, Singapore
[+] Present address: Singapore University of Technology and Design, 20 Dover Drive, Singapore 138682, Singapore

DOI: 10.1002/adfm.201101970

of around 150 μC cm^{-2}.[12] From theoretical calculations, this super-tetragonal phase was identified as a stable phase only under high compressive strain of above approximately 4.5%.[12] However, this super-tetragonal phase was first reported[16] to occur in a undoped BFO film deposited at high growth rate on STO substrates, which could not provide enough high compressive strain to trigger a stable giant tetragonal phase according to first principles calculations. Our recent investigation confirmed that increasing the growth rate of BFO films on STO substrates could induce a phase transition from monoclinic to giant tetragonal.[17] The origin of forming BFO super-tetragonal phase on STO substrate has never been studied and is still unclear. As detailed in the discussion below, by using high resolution synchrotron X-ray diffraction, atomic force microscopy (AFM), and transmission electron microscopy (TEM), the parasitic β-Bi_2O_3 (BO) phase is found to coexist with super-tetragonal BFO phase in BFO film grown at sputtering power of 180 W. By comparing the BFO films grown with and without BO buffer layer at low growth rate on SRO/STO substrates, the BO phase is identified to strongly associate with the stabilization of super-tetragonal BFO phase. In addition, we have built a structure model to provide details on the lattice mismatch and strain accommodation between the BO phase and BFO giant tetragonal phase. Furthermore, we have performed ab initio calculations, which show that the super-tetragonal BFO phase exhibits a lower level of total energy than that of monoclinic BFO phase when BO phase is present. These results can help understand the high leakage measured for the BFO samples with giant c/a ratio, where it likely that a small amount of highly conductive BO phase is involved. This prevents the room temperature measurement of giant polarization as predicted theoretically.[18]

2. Results

To check the possible phases present in the BFO film grown at a sputtering power of 180 W on SRO/STO substrate, high resolution X-ray diffraction scan along the L direction around (002) in the reciprocal space was measured from L-values of 1 to 2 (**Figure 1**a). In addition to the diffraction peaks from STO, SRO, and BFO, a peak at L = 1.43 was clearly shown, which corresponds to (002) lattice spacing of β-BO phase. The L scan around (–103) also gives rise to the peak from this phase at L = 2.14 (Figure 1b). (–103) Φ scans shown in Figure 1c–f reveal the in-plane epitaxial relationship between BFO, BO, SRO, and STO, demonstrating a four-fold symmetry. To establish a detailed crystal structure of this BO phase, reciprocal space mappings (RSM) were measured, shown in **Figure 2**. In the HL (002) RSM (Figure 2a), a horizontally elongated peak of BO phase is shown to exist at $L \approx 1.43$, which is similar to the (002) RSM from BFO. This suggests an intimate contact between BFO and BO lattice in the film with a large degree of out-of-plane orientation. From a single peak in (–103) RSM (Figure 2b), the BO phase was identified as a tetragonal β-BO with lattice parameters a = 7.913(2), c = 5.462(1) Å.

The presence of BO phase at high growth rate but not at low rate can be understood as follows. As the growth rate increases, more Bi would be stabilized as BO phase in the films due to more Bi atoms being sputtered with less time allowed for evaporation. BFO films grown at very high oxygen pressure also show the existence of BO phase in previous reports;[19,20] In

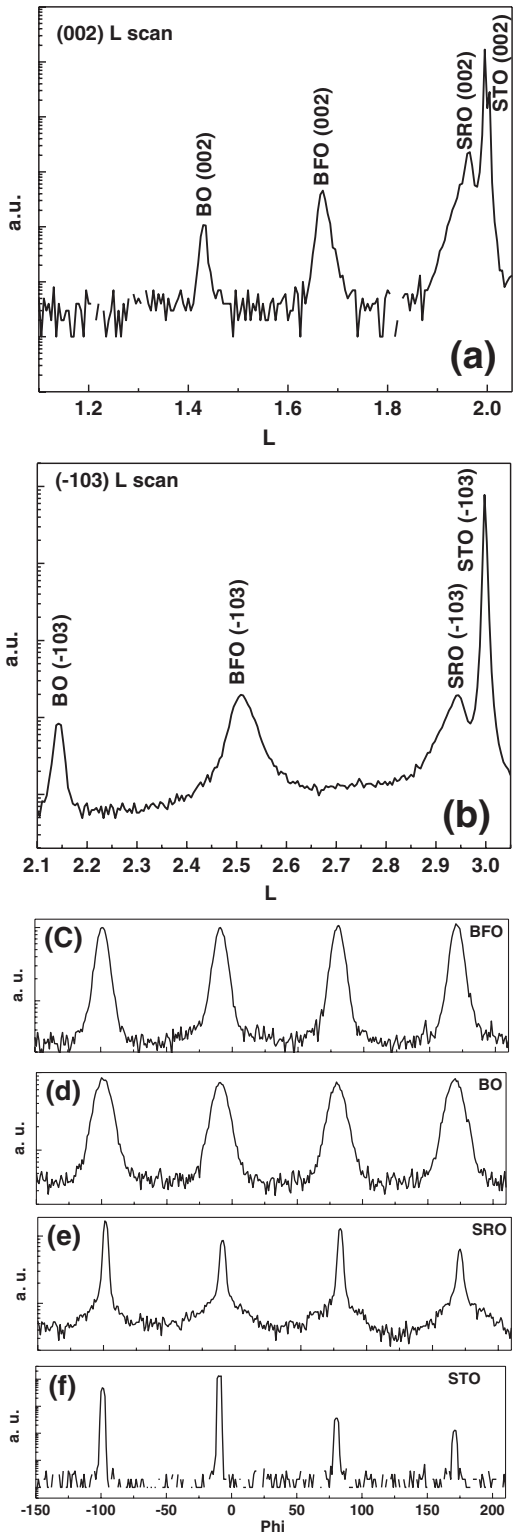

Figure 1. High resolution X-ray diffraction L scans around diffraction peaks of (002) (a) and (–103) (b). (–103) Φ scans of BFO (c), BO (d), SRO (e), and STO (f) lattice for the BFO film sputtered at 180 W on SRO/STO substrate.

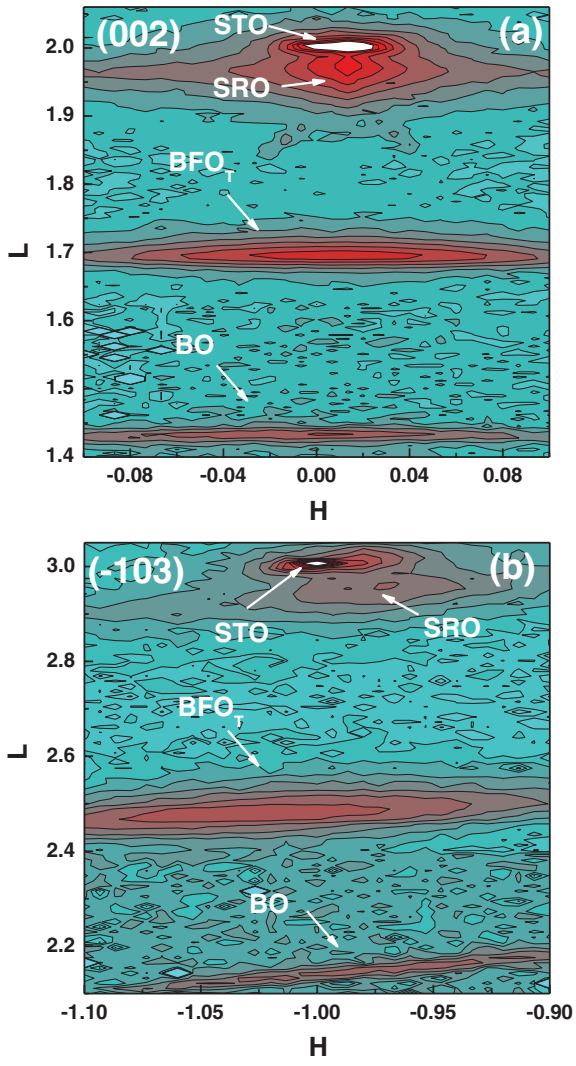

Figure 2. a) (002) *HL*, b) (–103) *HL* reciprocal space mappings of BFO film sputtered at 180 W on SRO/STO substrate.

both of these reported works (see Figure 4(a) in Bea et al.[19] and Figure 1 in You et al.[20]), there is an unidentified peak in the X-ray diffraction (XRD) spectrum at $2\theta \approx 39°$, corresponding to the (002) peak of super-tetragonal BFO phase. In our previous work,[17] for BFO films sputtered at power of 150 W, a weak XRD peak attributed to the BO phase was also observed, in addition to the strong peaks of the two tetragonal phases of BFO (not shown). Therefore, the super-tetragonal BFO phase was indeed in coexistence with the BO phase on STO substrates. In addition, the BO phase shares the same tetragonal symmetry with a reasonable lattice mismatch with super-tetragonal BFO phase. These obervations lead us to speculate of the possible function of BO phase in inducing the formation of super-tetragonal BFO phase.

In order to confirm the role the BO phase played in triggering the formation of super-tetragonal BFO phase, BFO film of 180 nm thickness was grown on BO buffered SRO/STO substrate at a sputtering power of 120 W. This growth rate has previously been demonstrated to lead to monoclinic M_A phase for BFO film deposited on SRO/STO substrate without BO buffer layer.[8] As shown in **Figure 3**a the BFO film grown with BO buffer layer shows a (002) peak corresponding to the super-tetragonal phase (thick line) while the film grown directly on SRO buffered STO substrate shows a (002) peak with lattice spacing of monoclinic phase (thin line). The *L* scan around (–103) in Figure 3b also confirms the super-tetragonal phase being induced in the BFO film deposited on BO buffer layer. HL reciprocal space mappings of (002) (Figure 3c) and (–103) (Figure 3d) were measured to determine the detailed structure of the BO buffered BFO film grown on SRO/STO substrate. In both mappings, the BFO phase shows a single peak, indicating a tetragonal symmetry. Also, the BO phase shows the same tetragonal symmetry as in the BFO film grown at 180 W in Figure 2. The lattice parameters for BO buffer layer are a = 8.230(2), c = 5.397(1) Å, while those for the BFO phase are a = 3.782(2), c = 4.681(1) Å.

In the following part of this work, the real space arrangement of BFO phase and BO phase in a 180 W sample is studied using AFM and cross-section TEM to clarify how BO phase can stabilize the super-tetragonal BFO phase on STO substrate. The in-plane AFM image (**Figure 4**a) shows a large amount of square-like outgrowth from the surface of BFO film sputtered at 180 W. This outgrowth was also shown in a previous report of BO excess films.[21] From the TEM cross-section image (Figure 4b), the outgrowth island is about 40 nm in height. For the elementary distribution in the film, EDX mappings (Figure 4c–e) reveal that the element Bi covers both the film and outgrowth island while the element Fe shows a lower intensity at the interface between the film and island. Therefore, the island outgrowth is introduced by BO phase presented in the film. At the BFO/SRO interface, the Bi element shows a higher intensity than Fe. This implies that BO phase acts as an inducing layer for BFO super-tetragonal phase in the film sputtered at 180 W.

The result of BFO lattice derived from high resolution TEM of the film sputtered at 180 W on SRO/STO substrate agrees well with that of the XRD result, i.e., $c \approx 4.6$ Å, as shown in **Figure 5**a. The single-crystal-like lattice of BO phase (Figure 5b) in the BFO film grown at 180 W is also consistent with XRD data. Two types of relationship between BO phase and BFO super-tetragonal phase were generally found in the film, which is consistent with EDX mappings. One is the existence of BO phase at the BFO/SRO interface (Figure 5c), acting as a buffer layer for the growth of BFO super-tetragonal phase. The other one is BO phase being sandwiched between BFO phases, leading to the formation of island outgrowths at the film surface, as shown in Figure 5d. A further common phenomenon is that dislocations and disorders of atomic arrangement occur around the region of BO phase to accommodate the lattice mismatches, which can be seen around the dashed lines in the TEM images of Figure 5c,d.

Based on the XRD and TEM results, a structure model is proposed to clarify the arrangement of BFO lattice with BO phase in the BFO film. The tetragonal β-BO lattice, as outlined with *a*, *b*, and *c* axes in **Figure 6**a, has a 45° in-plane relationship with the cubic δ-BO lattice. As the in-plane lattice parameter of super-tetragonal BFO phase (a = 3.779 Å) is about half that of the β-BO phase (a = 7.913 Å), there would be four unit cells of BFO lattice on one unit cell of BO lattice. One of the BFO unit

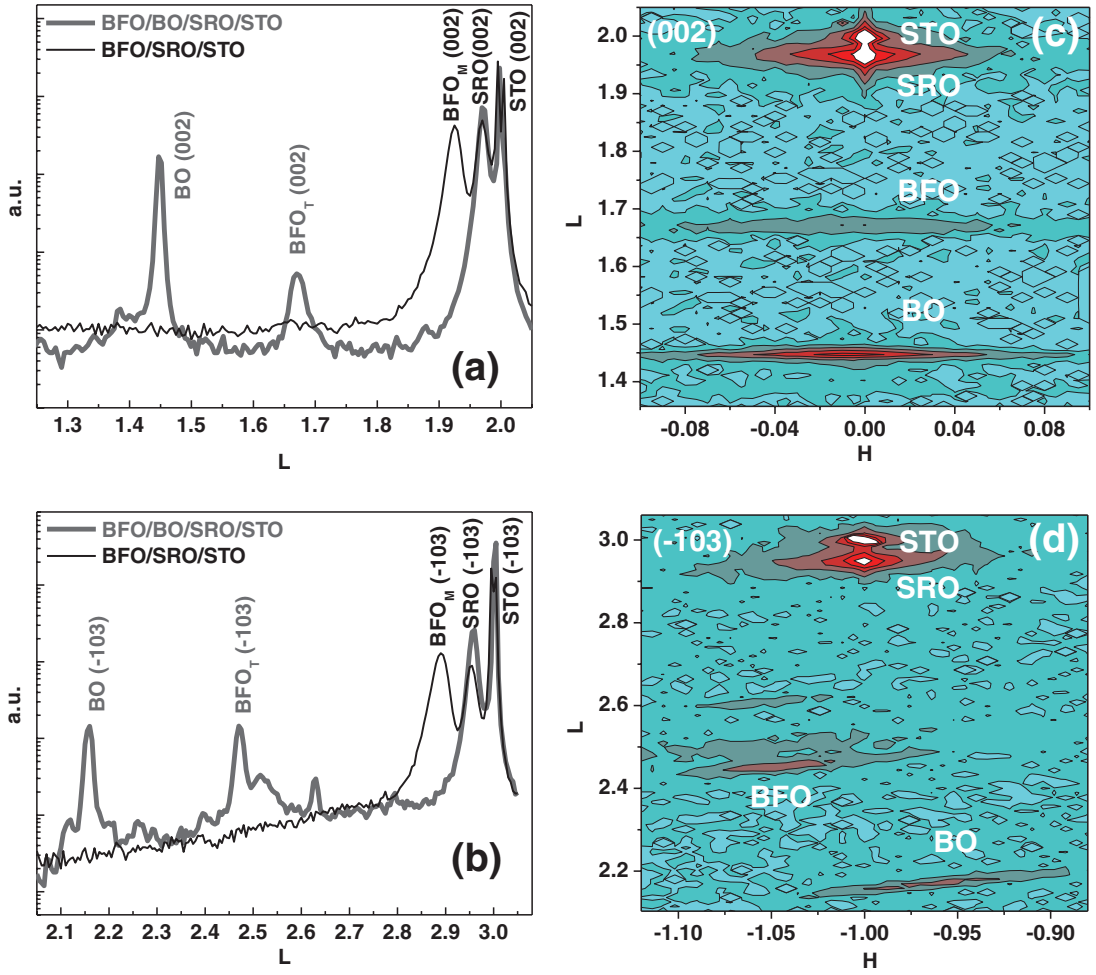

Figure 3. High resolution L scans of (002) (a), and (–103) (b) for BFO thin films grown at 120 W with (thick lines) and without BO (thin lines) buffer layer on SRO/STO substrate. c) (002) *HL*, and, d) (–103) *HL* reciprocal space mappings of 120 W BFO film grown with BO buffer layer on SRO/STO substrate.

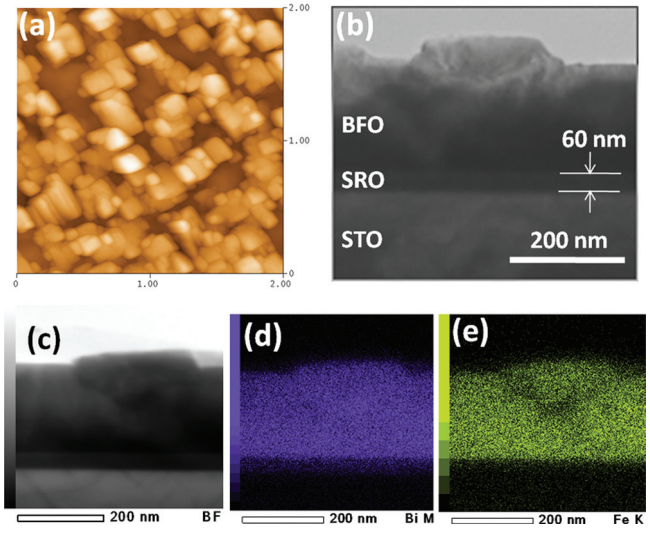

Figure 4. a) In-plane AFM image with the scan area 2 by 2 µm. b) Cross-section TEM image and c–e) EDX mappings with image (c), Bi M edge (d) and Fe K edge (e) of the BFO film sputtered at 180 W on SRO/STO substrate.

cells is drawn in Figure 6a. The cross-section view of the SRO/BO/BFO lattice in the *ac* plane is shown in Figure 6b. The in-plane lattice mismatch between SRO (a = 3.962 Å) and BO is only around 0.1%. Therefore the BO phase can easily grow epitaxially on SRO/STO substrate. Although the lattice mismatch between BO and super-tetragonal BFO is about 4.5%, which is quite large for epitaxial growth, experimentally it was found that BO phase prompts the formation of BFO super-tetragonal phase rather than monoclinic phase on STO substrates.

To further understand the stability of BFO phase in the presence of BO, we performed ab initio calculations within the PBE-GGA approximations[22] by using the full potential linear augmented plane wave (FP-LAPW) as implemented in the WIEN2K software package.[23] This allows us to compute the electronic structure of BFO within DFT utilizing the full potential (linear) augmented plane wave plus local orbitals (APW+lo) method. For the atomic sphere radii we chose values of 2.3, 1.9, and 1.45 au for Bi, Fe, and O, respectively. Inside the atomic spheres, the partial waves were expanded up to l_{max} = 10 and the number of plane waves was cut off at $R_{MT}K_{max}$ = 7.0. The charge density was Fourier-expanded with G_{max} = 14 Ry. A

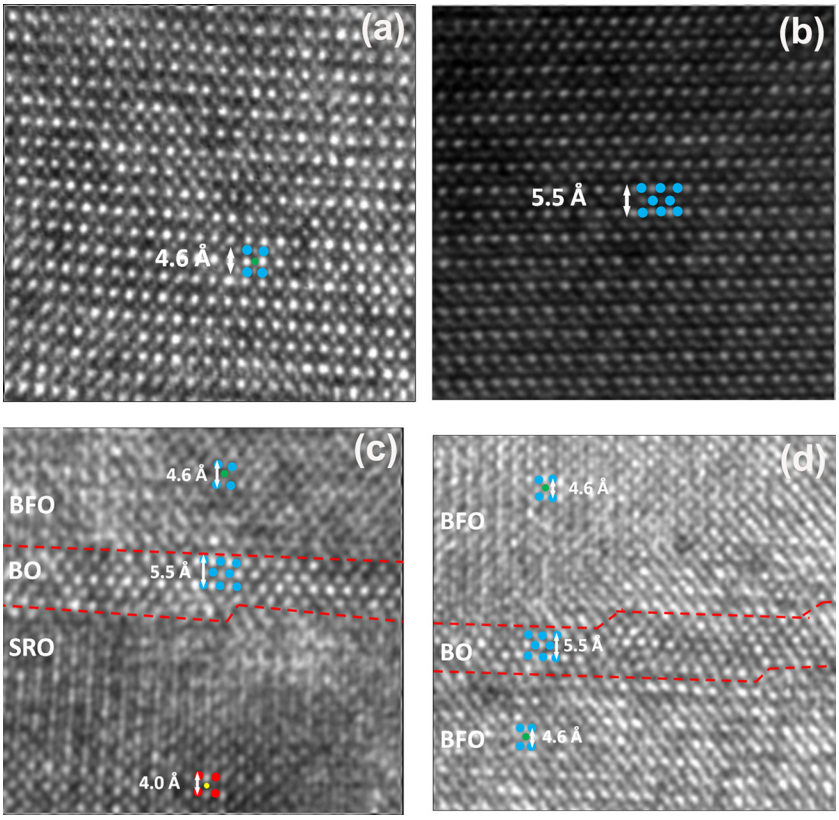

Figure 5. High resolution bright field TEM images of the BFO super-tetragonal lattice (a) and BO lattice (b) in film sputtered at 180 W on SRO-buffered STO substrate. c) BO lattice at the BFO/SRO interface. d) BO lattice sandwiched between BFO super-tetragonal lattices.

k-mesh of $6 \times 6 \times 6$ k-points in the full Brillouin zone was used. In addition to the usual valence states, extra local orbitals for "semi-core" states (Bi – 5p, 5d, 6s; Fe – 3s, 3p; and, O – 2s) were also added and considered as band states.

We looked at the three different G-type anti-ferromagnetic structures of BFO: i) the tetragonal structure with lattice parameters of $a = b = 3.780$ Å, and $c = 4.677$ Å with ratio $c/a = 1.237$, as experimentally observed above; ii) the tetragonal structure with lattice constant being half of the β-BO or $a = b = 3.956$ Å and the c/a ratio being the same as for structure (i); and, iii) the monoclinic structure, that was obtained when we directly grow BFO on the SRO-buffered STO substrate,[8] with $a\sqrt{2} = 5.612$ Å; $b\sqrt{2} = 5.602$ Å, and $c = 4.057$ Å, $\alpha = 90°$, $\beta = 89.53°$, $\gamma = 90°$. We found that the tetragonal structures, structure (i) and (ii) are more stable than the monoclinic structure, structure (iii), with energy differences $\Delta E_1 = E_i - E_{iii} = -18.97$ mRy per f.u, $\Delta E_2 = E_{ii} - E_{iii} = -5.07$ mRy per formula unit (f.u.), here E_i, E_{ii}, and E_{iii} are the total energies of structures (i), (ii), and (iii), respectively.

For tetragonal structures, at each of constrained lattice constants a, we examined the energy with different c/a ratios. We found that for constrained BFO at $a = 3.780$ Å, structure (i), the lattice constant $c = 4.677$ Å corresponds to a compressive strain of 3.48% along the c-axis in comparison to the most theoretical stable structure at $c/a = 1.28$, see **Figure 7**a. For constrained BFO at $a = 3.956$ Å, our simulation shows the most stable tetragonal structure is at $c/a = 1.16$, see Figure 7b. In comparison to the tetragonal structure with $a = 3.956$ Å and $c/a = 1.16$, structure (i) is still more stable with energy difference, $\Delta E = E_i - E(a = 3.956$ Å, $c/a = 1.16) = -7.24$ mRy per f.u. This supports the experimental observation that the tetragonal structure, structure (i), with $a = b = 3.780$ Å, and $c = 4.677$ Å is the most stable structure, in the presence of BO.

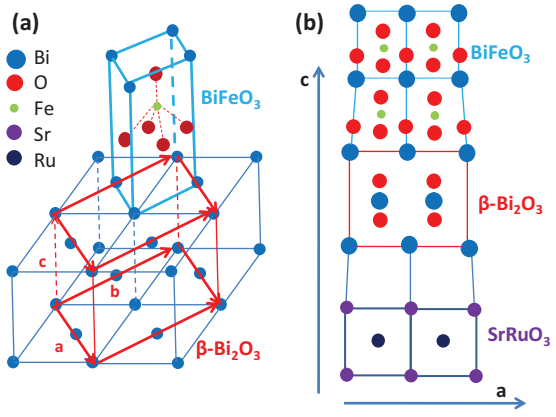

Figure 6. a) Three-dimensional schematic interface structure model for BFO and BO lattice, the oxygen atoms in the BO lattice were not included for easier visualization. b) Cross-section view of the SRO/BO/BFO lattice in the ac plane.

3. Conclusions

By detailed structure analyses using high resolution synchrotron X-ray diffraction, the parasitic β-BO phase is identified to coexist with the super-tetragonal BFO phase in BFO film deposited at sputtering power of 180 W on SRO/STO substrate. At a fixed sputtering power of 120 W, the BFO film grown directly on SRO/STO substrate shows a monoclinic phase, whereas the BFO film deposited on BO buffered SRO/STO substrate demonstrates a super-tetragonal phase. This confirms that the parasitic β-BO phase is largely responsible for the formation of super-tetragonal BFO phase in the film deposited on STO substrates. By combined AFM and TEM studies, the detailed arrangement of β-BO phase and super-tetragonal BFO phase in the film is clarified. This leads to a schematic interfacial structure model to explain the lattice mismatch and strain accommodation in the multiphase film. Our ab initio calculations support the experimental observation that the super-tetragonal BFO phase is more stable than monoclinic phase when BO is present. As BO phase is known to be highly conductive,[21,24] it could act as a bottom electrode and buffer layer of inducing super-tetragonal BFO phase at the same time. This opens an alternative formation route for the super-tetragonal BFO phase on single crystal substrates (for example, STO) and even

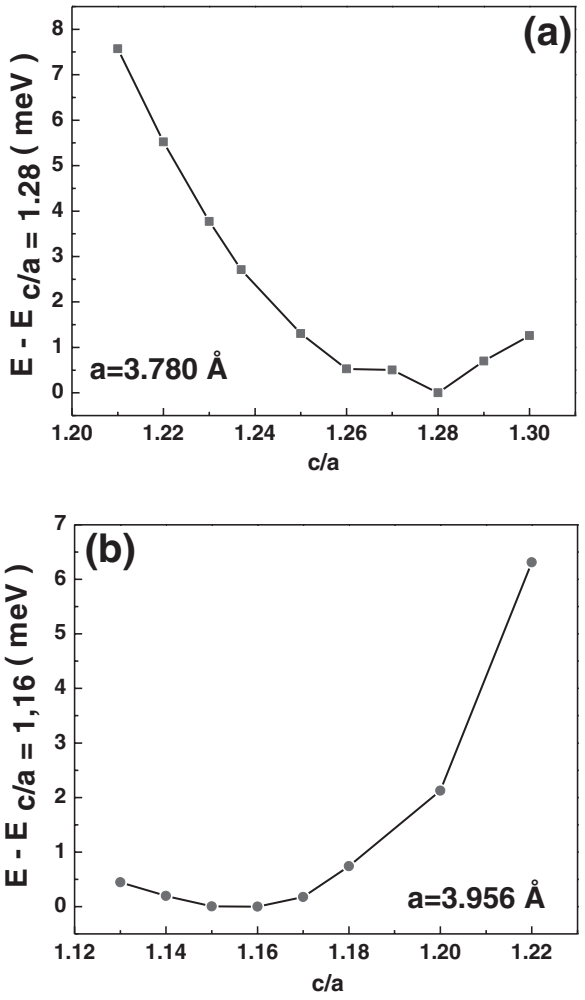

Figure 7. The total energy difference of tetragonal antiferromagnetic BFO as a function of c/a ratio for two different constrained a parameters: a) $a = 3.780$ Å with the total energy relative to the most stable structure at $c/a = 1.28$; and, b) $a = 3.956$ Å with the total energy relative to the most stable state at $c/a = 1.16$.

polycrystalline substrates, as long as the BO phase is properly controlled as a buffer layer.

4. Experimental Section

Epitaxial BFO (001) films with fixed thickness of around 180 nm were deposited at sputtering power from 30 to 180 W on STO substrates by radio-frequency sputtering.[25] To demonstrate the effect of BO, BFO film of 180 nm in thickness was grown on BO buffered SRO/STO substrate at a sputtering power of 120 W. BO ceramic polycrystalline target was made by sintering at 600 °C for 2 h. The crystal structures of BFO films with and without BO buffer layer were identified using high resolution synchrotron X-ray diffractometry at the XDD (X-ray Development and Demonstration) beam line of Singapore Synchrotron Light Source (SSLS) and Shanghai Synchrotron Radiation Facility (SSRF). AFM (Digital Instruments) was used to study the surface morphology. Cross-sectional TEM studies were made by using Philips CM300 FEG TEM at an acceleration voltage of 300 kV and the energy dispersive X-ray spectroscopy (EDX) analysis was obtained from scanning transmission electron microscopy (STEM) detector on a JEOL JEM-2010F at 200 kV.

Acknowledgements

The authors are grateful for technical support received at beamline BL14B1 (diffractometry) of SSRF for the data collection under project nos. j11sr0029 and 09sr0157. P.Y. is grateful for support from SSLS via NUS Core Support C-380-003-003-001. J.W. acknowledges the grant support of MOE, Singapore Ministry of Education Academic Research Fund Tier 1 (Grant Number: T11-0702-P06, R-284-000-054-112), conducted at National University of Singapore. The authors acknowledge the support at the Institute of Materials Research and Engineering, A-STAR, through project IMRE/10-1C0109 and Tan Hui Ru for help with TEM.

Received: August 21, 2011
Revised: October 8, 2011
Published online: December 21, 2011

[1] R. Ramesh, N. A. Spaldin, *Nat. Mater.* **2007**, *6*, 21.
[2] G. Catalan, J. F. Scott, *Adv. Mater.* **2009**, *21*, 2463.
[3] T. Zhao, A. Scholl, F. Zavaliche, K. Lee, M. Barry, A. Doran, M. P. Cruz, Y. H. Chu, C. Ederer, N. A. Spaldin, R. R. Das, D. M. Kim, S. H. Baek, C. B. Eom, R. Ramesh, *Nat. Mater.* **2005**, *5*, 823.
[4] W. Ji, K. Yao, Y. C. Liang, *Adv. Mater.* **2010**, *22*, 1763.
[5] D. G. Schlom, L.-Q. Chen, C.-B. Eom, K. M. Rabe, S. K. Streiffer, J.-M. Triscone, *Annu. Rev. Mater. Res.* **2007**, *37*, 589.
[6] F. Kubel, H. Schmid, *Acta Cryst. B* **1990**, *46*, 698.
[7] K. Saito, A. Ulyanenkov, V. Grossmann, H. Ress, L. Bruegemann, H. Ohta, T. Kurosawa, S. Ueki, H. Funakubo, *Jpn. J. Appl. Phys.* **2006**, *45*, 7311.
[8] H. Liu, K. Yao, P. Yang, Y. Du, Q. He, Y. Gu, X. Li, S. Wang, X. Zhou, J. Wang, *Phys. Rev. B* **2010**, *82*, 064108.
[9] H. M. Christen, J. H. Nam, H. S. Kim, A. J. Hatt, N. A. Spaldin, *Phys. Rev. B* **2011**, *83*, 144107.
[10] D. Mazumdar, V. Shelke, M. Iliev, S. Jesse, A. Kumar, S. V. Kalinin, A. P. Baddorf, A. Gupta, *Nano Lett.* **2010**, *10*, 2555.
[11] M. N. Iliev, M. V. Abrashev, D. Mazumdar, V. Shelke, A. Gupta, *Phys. Rev. B* **2010**, *82*, 014107.
[12] A. J. Hatt, N. A. Spaldin, C. Ederer, *Phys. Rev. B* **2010**, *81*, 054109.
[13] Z. Chen, S. Prosandeev, Z. L. Luo, W. Ren, Y. Qi, C. W. Huang, L. You, C. Gao, I. A. Kornev, T. Wu, J. Wang, P. Yang, T. Sritharan, L. Bellaiche, L. Chen, *Phys. Rev. B* **2011**, *84*, 094116.
[14] B. Dupe, S. Prosandeev, G. Geneste, B. Dkhil, L. Bellaiche, *Phys. Rev. Lett.* **2011**, *106*, 237601.
[15] R. J. Zeches, M. D. Rossell, J. X. Zhang, A. J. Hatt, Q. He, C. H. Yang, A. Kumar, C. H. Wang, A. Melville, C. Adamo, G. Sheng, Y. H. Chu, J. F. Ihlefeld, R. Erni, C. Ederer, V. Gopalan, L. Q. Chen, D. G. Schlom, N. A. Spaldin, L. W. Martin, R. Ramesh, *Science* **2009**, *326*, 977.
[16] D. Ricinschi, K.-Y. Yun, M. Okuyama, *J. Phys.: Condens. Matter* **2006**, *18*, L97.
[17] H. Liu, P. Yang, K. Yao, J. Wang, *Appl. Phys. Lett.* **2011**, *98*, 102902.
[18] H. Bea, B. Dupe, S. Fusil, R. Mattana, E. Jacquet, B. Warot-Fonrose, F. Wilhelm, A. Rogalev, S. Petit, V. Cros, A. Anane, F. Petroff, K. Bouzehouane, G. Geneste, B. Dkhil, S. Lisenkov, I. Ponomareva, L. Bellaiche, M. Bibes, A. Barthelemy, *Phys. Rev. Lett.* **2009**, *102*, 217603.
[19] H. Bea, M. B. S. Fusil, K. Bouzehouane, E. Jacquet, K. Rode, P. Bencok, A. Barthelemy, *Phys. Rev. B* **2006**, *74*, 020101(R).
[20] L. You, N. T. Chua, K. Yao, L. Chen, J. Wang, *Phys. Rev. B.* **2009**, *80*, 024105.
[21] H. Bea, M. Bibes, A. Barthelemy, K. Bouzehouane, E. Jacquet, A. Khodan, J.-P. Contour, S. Fusil, F. Wyczisk, A. Forget, D. Lebeugle, D. Colson, M. Viret, *Appl. Phys. Lett.* **2005**, *87*, 072508.
[22] J. P. Perdew, K. Burke, M. Ernzerhof, *Phys. Rev. Lett.* **1996**, *77*, 3865.
[23] P. Blaha, K. Schwarz, G. K. H. Madsen, D. Kvasnicka, J. Luitz, *WIEN2k, An Augmented Plane Wave plus Local Orbitals Program for Calculating Crystal Properties*, Karlheinz Schwarz, TU Vienna, Austria **2001**.
[24] T. Takahashi, H. Iwahara, *Mater. Res. Bull.* **1978**, *13*, 1447.
[25] H. Liu, P. Yang, K. Yao, J. Wang, *Appl. Phys. Lett.* **2010**, *96*, 012901.